HHS Public Access

Author manuscript

J Am Chem Soc. Author manuscript; available in PMC 2018 March 01.

Published in final edited form as:

J Am Chem Soc. 2017 March 01; 139(8): 3161–3170. doi:10.1021/jacs.6b12861.

N–H Bond Dissociation Enthalpies and Facile H Atom Transfers for Early Intermediates of Fe–N_2 and Fe–CN Reductions

Jonathan Rittle and **Jonas C. Peters**

Division of Chemistry and Chemical Engineering, California Institute of Technology (Caltech), Pasadena, California 91125, United States

Abstract

Fe-mediated biological nitrogen fixation is thought to proceed via either a sequence of proton and electron transfer steps, concerted H atom transfer steps, or some combination thereof. Regardless of the specifics and whether the intimate mechanism for N_2-to-NH_3 conversion involves a distal pathway, an alternating pathway, or some hybrid of these limiting scenarios, Fe–N_xH_y intermediates are implicated that feature reactive N–H bonds. Thermodynamic knowledge of the N–H bond strengths of such species is scant, and is especially difficult to obtain for the most reactive early stage candidate intermediates (e.g., Fe–N=NH, Fe=N–NH_2, Fe–NH=NH). Such knowledge is essential to considering various mechanistic hypotheses for biological (and synthetic) nitrogen fixation and to the rational design of improved synthetic N_2 fixation catalysts. We recently reported several reactive complexes derived from the direct protonation of Fe–N_2 and Fe–CN species at the terminal N atom (e.g., Fe=N–NH_2, Fe–C≡NH, Fe≡C–NH_2). These same Fe–N_2 and Fe–CN systems are functionally active for N_2-to-NH_3 and CN-to-CH_4/NH_3 conversion, respectively, when subjected to protons and electrons, and hence provide an excellent opportunity for obtaining meaningful N–H bond strength data. We report here a combined synthetic, structural, and spectroscopic/analytic study to estimate the N–H bond strengths of several species of interest. We assess the reactivity profiles of species featuring reactive N–H bonds and estimate their homolytic N–H bond enthalpies via redox and acidity titrations. Very low N–H bond dissociation enthalpies ($BDE_{N–H}$), ranging from 65 (e.g., Fe–C≡NH) to ≤37 kcal/mol (Fe–N=NH), are determined. The collective data presented herein provides insight into the facile reactivity profiles of early stage protonated Fe–N_2 and Fe–CN species.

Graphical abstract

Correspondence to: Jonas C. Peters.

Supporting Information: The Supporting Information is available free of charge on the ACS Publications website at DOI: 10.1021/jacs.6b12861., Crystallographic data (CIF), Detailed experimental procedures and spectroscopic and theoretical data (PDF),

The authors declare no competing financial interest.

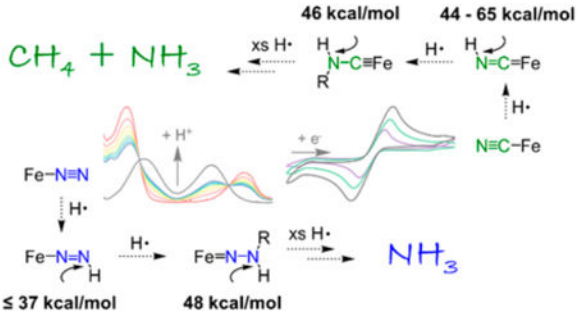

Introduction

The conversion of N_2 to NH_3 via reductive protonation by six electrons and protons is a fascinating transformation that is distinct from the Haber–Bosch process[1] and may offer a conceptual pathway for direct, distributed solar-driven ammonia synthesis.[2] Free N_2 exhibits a low electron affinity (−1.9 eV) and proton affinity (118 kcal/mol),[3] and activation by a suitable catalyst is hence required. While growing in number,[4] few well-defined molecular systems mediate catalytic N_2-to-NH_3 conversion; those that do use a combination of inorganic reductant and acid rather than H_2. Nitrogenase enzymes represent the most efficient and well-studied non-Haber–Bosch catalysts and are collectively responsible for the generation of ~50% of the global fixed nitrogen pool.[5] These enzymes sustain life and provide proof-of-concept that reductive protonation of N_2 can be carried-out under ambient conditions on a grand scale. But we do not as yet have a clear mechanistic picture of this biological transformation.

Well-defined inorganic model complexes that catalyze N_2-to-NH_3 conversion are particularly well suited to mechanistic investigations and a number of synthetic systems featuring early transition metals (especially Mo) have been studied in the context of N_2 activation[6] and catalytic N_2-to-NH_3 conversion.[4] An early hallmark of the Mo model systems, noteworthy owing to the presence of Mo in the FeMo-cofactor of MoFe-nitrogenase, has been the ability to independently prepare many of the intermediate Mo–N_xH_y species thought to be relevant to N_2-to-NH_3 conversion.[7]

Fe is an essential element in all known nitrogenases, and there is growing evidence that it plays a critical mechanistic role in the key bond-making and breaking events of overall N_2-to-NH_3 conversion.[5,8] For example, structural, spectroscopic, and theoretical evidence implicate the involvement of one (or more) of the iron atoms of the FeMo-cofactor in substrate binding/activation.[8] This state of affairs has motivated the study of well-defined Fe–N_xH_y species relevant to N_2 activation chemistry. In this context, Holland and Murray have for instance independently demonstrated that β-diketiminate-supported iron systems enable the delivery of electron equivalents to N_2 to generate bridging Fe-nitrido and/or imido species.[9,10] N_2-derived NH_3 can then be released from these systems upon subsequent protonation.[9b]

Our lab has reported several Fe systems that catalyze N_2-to-NH_3 conversion,[11] and we have very recently reported on a related (but as yet only stoichiometric) reductive protonation of

Fe–CN to release CH_4 and NH_3.[12] Interest in this subfield is growing. Very recently, Nishibayashi and co-workers disclosed a phosphine–pyrrole Fe–N_2 system that is a competent catalyst for NH_3 generation (along with some N_2H_4),[4a] and Ashley and co-workers reported a low-valent phosphine-only Fe–N_2 system that mediates catalytic N_2-to-N_2H_4 conversion.[4b] Fe-mediated, catalytic N_2 activation in these Fe systems is thought to involve an initial end-on binding of N_2 to a single Fe atom, followed (in our P_3^EFe-systems at least (E = B, C, Si)) by reductive protonation at the terminal N atom to afford Fe=N–NH_2 species (Scheme 1).[13] Fe-mediated reduction of P_3^{Si}Fe–CN is thought to proceed via an isostructural Fe≡C–NH_2 species.[12] These species are characteristic of a “distal” or “Chatt-type” pathway for substrate reduction that is commonly thought to operate in certain N_2 reduction systems. [3,4,7] Recent mechanistic studies of one of our reported Fe systems (P_3^{Si}Fe) also hints at competing downstream pathways following the generation of the doubly protonated distal intermediate P_3^{Si}Fe=N–NH_2. These Fe=N–NH_2 (and related Fe≡C–NH_2) species display a high degree of instability in comparison to analogous Mo=N–NH_2 species; for instance, they decay rapidly at ambient and even lower temperatures in solution and furnish mixtures of H_2 and NH_3. Understanding the factors that govern their reactivity patterns is critical from a mechanistic perspective and will aid in the development of improved catalysts that show better selectivity for NH_3 versus H_2. We anticipate that the high degree of reactivity observed in certain Fe–N_xH_y (and Fe–CNH_x) species must be correlated with unusually weak N–H bonds; this should be especially true of the first protonated species, Fe–N=NH (and Fe-C≡NH).[14] These weak N–H bonds might then serve a dual role: they could be susceptible to undesirable H_2 formation pathways that short circuit overall substrate reduction, while concomitantly facilitating downstream H atom-transfer pathways that productively lead to reduced product.

Whereas the thermochemistry of N–H bond formation in certain Ti-, Zr- and Mo-containing scaffolds operative in stoichiometric NH_3 formation has been recently studied,[15] such information is generally scant, and we saw an opportunity to map the N–H bond strengths of the most highly reactive species relevant to Fe-mediated N_2-to-NH_3 (and CN^-) conversion catalysis. In this report, we investigate H^+/e^- transfer to several Fe–CN- and Fe–N_2-derived species using the tripodal tris(phosphino)silyl ligand, P_3^{Si} (P_3^{Si} = [(2-*i*Pr$_2$P–C_6H_4)$_3$Si]$^-$; Scheme 1). While the P_3^{Si}Fe–N_2 system is not as active as its P_3^BFe-cousin for N_2-to-NH_3 conversion, it does mediate NH_3 generation and is technically better suited to the types of studies detailed here. Similarly, the P_3^{Si}Fe–CN system is competent for NH_3 and CH_4 generation[12] and offers a number of advantages in terms of measuring N–H bond strengths, including experimental access to the first protonated intermediate (P_3^{Si}Fe–C≡$NH^{+/0}$) and well-behaved redox and acid–base properties.

Results and Discussion

N–H Bond Strength of P_3^{Si}Fe–C≡$NH^{0/+}$

While the conversion of Fe–N_2 to an Fe–N_xH_y species could in principle be mediated by HAT steps, most commonly used H atom donor reagents are not sufficiently reactive to donate H atoms to Fe–N_2 precursors.[16] The same is true of Fe–CN species.[12] Consistent with this statement, there is no reaction between either P_3^{Si}Fe–N_2 or P_3^{Si}Fe–CN with 9,10-

dihydroanthracene (BDE_{CH} = 81 kcal/mol) or TEMPOH (BDE_{CH} = 71 kcal/mol) within 1 h at room temperature in THF solution (Scheme 2).[17] This observation suggests (but does not require) that the $BDE_{N–H}$ values for the corresponding $P_3^{Si}Fe{=}C{=}NH$ and $P_3^{Si}Fe–N{=}NH$ species are <70 kcal/mol. For comparison, the experimentally determined $BDE_{N–H}$ of diazene, HN=NH, is ~61 kcal/mol.[18] Interestingly, an immediate reaction is observed upon combining $[P_3^{Si}Fe–C{\equiv}NH][BAr^F{}_{24}]$[12] with 1 equiv of TEMPO● to form $[P_3^{Si}Fe–CN][BAr^F{}_{24}]$ and TEMPOH (Scheme 2). This latter observation indicates that the homolytic bond dissociation free energy (BDFE) or bond dissociation enthalpy (BDE) of the N–H bond in $[P_3^{Si}Fe–C{\equiv}NH][BAr^F{}_{24}]$ is significantly lower than that of the $BDE_{O–H}$ or $BDFE_{O–H}$ in TEMPOH.

The prolonged THF solution stability of $P_3^{Si}Fe–CN$, $P_3^{Si}Fe–CN^+$, $P_3^{Si}Fe–C{\equiv}NH^+$, and mixtures thereof permits the collection of data that can then be used to quantify the $BDE_{N–H}$ of $P_3^{Si}Fe–C{\equiv}NH^+$. The solution $BDE_{N–H}$ is proportional to the sum of the acidity of the relevant N–H bond (pK_a) and the oxidation potential (E°_{ox}) and may be estimated by the application of eq 1 or 2,

$$\mathrm{BDE(N{-}H^{+})}=23.06E_{\mathrm{ox}}(N)+1.37\mathrm{p}K_{\mathrm{a}}(\mathrm{N{-}H^{+}})+C_{\mathrm{H}} \quad (1)$$

$$\mathrm{BDE(N{-}H)}=23.06E_{\mathrm{ox}}(\mathrm{N{-}H})+1.37\mathrm{p}K_{\mathrm{a}}(\mathrm{N{-}H^{+}})+C_{\mathrm{H}} \quad (2)$$

where C_H is a solvent-dependent constant reported as 66 kcal/mol in THF.[17,19,20,] Cyclic voltammetry of $P_3^{Si}Fe–CN$ in a THF electrolyte (0.1 M $[TBA][PF_6]$) reveals a one-electron oxidation event at −0.38 versus the ferrocene/ferrocenium couple. $[P_3^{Si}Fe–C{\equiv}NH][BAr^F{}_{24}]$ displays a reduction event at −1.27 V under similar conditions (Figure 1). To determine the apparent acidity of $[P_3^{Si}Fe–C{\equiv}NH]^+$ in THF solution, titrations of $P_3^{Si}Fe–CN$ were performed with a series of acids and monitored by UV–visible spectroscopy. $P_3^{Si}Fe–CN$ does not detectably react with the acids $[HNEt_3][OTf]$ (pK_a 13.7) or [LutH][OTf] (pK_a 9.5); stoichiometric addition of the chlorinated anilinium salts $[2\text{-}Cl\text{-}PhNH_3][OTf]$ (pK_a = 6.0 in THF) or $[2,5\text{-}Cl_2\text{-}PhNH_3][OTf]$ (pK_a = 4.5 in THF) results in the formation of equilibrium mixtures of $P_3^{Si}Fe–CN$ and $[P_3^{Si}Fe–C{\equiv}NH][OTf]$ at room temperature (Figure 1).[21] Spectrophotometric titrations performed with these acids and $P_3^{Si}Fe–CN$ furnish an average pK_a = 5.6(1) for the acidic N–H proton of $[P_3^{Si}Fe–C{=}NH][OTf]$.

With these data in hand, the $BDE_{N–H}$ of $[P_3^{Si}Fe–C{\equiv}NH][OTf]$ and its one-electron reduced relative $P_3^{Si}Fe{=}C{=}NH$ may be estimated using eqs 1 and 2, respectively. These values are found to be 65(1) and 44(1) kcal/mol, respectively (Table 1), and are consistent with the complete and irreversible hydrogen atom abstraction reaction between $[P_3^{Si}Fe–C{\equiv}NH][BAr^F{}_{24}]$ and TEMPO● ($BDE_{O–H}$ = 71 kcal/mol), and the inability of $P_3^{Si}Fe–CN$ to react with TEMPOH or dihydroanthracene via hydrogen atom abstraction. The decrease by more than 20 kcal/mol in the N–H bond strength on going from cationic $[P_3^{Si}Fe–C{\equiv}NH]^+$ to neutral $P_3^{Si}Fe{=}C{=}NH$ is striking.

We think this dramatic difference is largely a consequence of varying degrees of C–N bond weakening that occur concomitant with H atom addition to the Fe–CN unit. Crystallographic studies indicate that in cationic $P_3^{Si}Fe–C{\equiv}NH^+$ a short C–N bond is observed (1.130(3) Å) and the N atom is largely sp-hybridized (∠CNH 176(3)°) (Table 2).[12] Density functional theory (DFT) calculations on the gas-phase optimized geometry of $P_3^{Si}Fe{=}C{=}NH$ predict an sp^2-hybridized N atom (∠CNH 126.6°) and a long C–N bond (1.233 Å) (Supporting Information). Comparison of these C–N bond lengths with the corresponding $P_3^{Si}Fe–CN^{+/0}$ species reveal that formal H atom addition to $P_3^{Si}Fe–CN^+$ results in minimal alteration to the C–N bond length (0.014 Å) whereas H atom addition to neutral $P_3^{Si}Fe–CN$ results in significant C–N bond lengthening (0.066 Å). Accordingly, the measured $BDE_{N–H}$ values reflect the extent to which the C≡N bond is weakened; weak N–H bonds are correlated with a HAT process that causes significant weakening of the C≡N (or N≡N) bond. Generally speaking, weak N–H bonds may be signatures of early stage intermediates of N_2/CN activation that are preceded by the most challenging H atom additions. Identifying these intermediates is critical to understanding the thermodynamic challenges associated with these difficult bond activation processes.

Monoprotonation of Fe–N_2

Terminally bound iron diazenido complexes (Fe–N=NH) have been invoked as the first intermediates of biological N_2 reduction[5b] and are likewise presumed to be reactive intermediates in stoichiometric and catalytic N_2-to-NH_3 reactions effected by $P_3^EFe–N_2$ (E = B, C, Si) and related systems.[11,13] Direct characterization of Fe–N=NH species has proven to be a significant challenge, and circumstantial observations suggest that the $BDFE_{N–H}$ or $BDE_{N–H}$ values for $P_3^EFe–N{=}NH^{0/+}$ intermediates are significantly lower than that of gas phase HN=NH (~61 kcal/mol)[18] but can be anticipated to be similar to, or perhaps less than, that estimated for $P_3^{Si}Fe{=}C{=}NH$ (44 kcal/mol). Given the comparatively high stability of the related monoprotonated cyanide complex, $[P_3^{Si}Fe–C{\equiv}NH][BAr^F{}_{24}]$, we wondered whether the N–H bond strength in isostructural $P_3^{Si}Fe–N{=}NH^+$ could be estimated. Although the oxidation potential of $P_3^{Si}Fe–N_2$ ($E°$ = −1.0 V) has been previously reported,[16] the weakly basic properties of $P_3^{Si}Fe–N_2$ prevents access to the needed pK_a data to directly estimate the $BDE_{N–H}$ for $P_3^{Si}Fe–N{=}NH^+$ in ethereal solvents. Nonetheless, several observations that place a firm upper limit on its $BDE_{N–H}$ are as follows.

The addition of stoichiometric quantities of chlorinated anilinium triflate salts or $[H(OEt_2)_2][BAr^F{}_{24}]$ to $P_3^{Si}Fe–N_2$ in THF at 298 K results in immediate oxidation to form $P_3^{Si}Fe–OTf$ and $[P_3^{Si}Fe–N_2][BAr^F{}_{24}]$, respectively, prohibiting further investigations at this temperature.[13,16] Combining solutions of $P_3^{Si}Fe–N_2$ with stoichiometric $[H(OEt_2)_2][BAr^F{}_{24}]$ (p$K_{a(THF)}$ ≈ 0)[22] at 173 K leads to the formation of EPR-silent $[P_3^{Si}Fe–N_2][BAr^F24]$ over 15 min, as determined by UV–visible spectroscopy. EPR analysis of freeze-quenched solutions of $P_3^{Si}Fe–N_2$ rapidly combined with 1–5 equiv of $[H(OEt_2)_2]$-$[BAr^F{}_{24}]$ shows unaltered EPR signatures for $P_3^{Si}–N_2$ remaining in the frozen reaction mixtures (Supporting Information). In contrast, the analogous protonation of isoelectronic $P_3^{Si}Fe{=}C{=}NMe$ to form the carbyne $[P_3^{Si}Fe{\equiv}C–N(Me)H][BAr^F{}_{24}]$ results in a significant change in the observed EPR signatures (vide infra). The aforementioned observations collectively establish that $P_3^{Si}Fe–N_2$ is not detectably protonated by $[H(OEt_2)_2][BAr^F{}_{24}]$ (at

the N atom or otherwise) at 173 K, and hence the pK_a of the putative $P_3^{Si}Fe–N=NH^+$ is ≤0 in THF solution. According to eq 1, an upper limit for the $BDE_{N–H}$ value of $P_3^{Si}Fe–N=NH^+$ can thereby be estimated at ≤43 kcal/mol. This value is significantly less than that experimentally determined for $P_3^{Si}Fe–C≡NH^+$ (65 kcal/mol). The DFT-optimized geometry of $P_3^{Si}Fe–N=NH^+$ indicates significant N–N bond weakening (by 0.12 Å) on H atom addition to $P_3^{Si}Fe–N_2^+$ that is likely correlated with a very weak N–H bond. (Table 2, Supporting Information).

In a similar context, our attempts to generate neutral $P_3^{Si}Fe–N=NH$ resulted in apparent disproportionation reactions. The addition of stoichiometric $[H(OEt_2)_2][BAr_{24}]$ to $P_3^{Si}Fe–N_2^-$ results in immediate one-electron oxidation to form $P_3^{Si}Fe–N_2$ when performed at ambient temperatures, with simultaneous formation of 0.5 mol equiv of H_2.[13b,16] We have re-examined this reaction at 138 K in thawing 2-MeTHF, and while an instantaneous color change is observed on combining $P_3^{Si}Fe–N_2^-$ with 1 equiv of either $[H(OEt_2)_2][BAr^F_{24}]$ or $[PhNH_3]$-[OTf], we do not observe the multinuclear NMR resonances we expect for $P_3^{Si}Fe–N=NH$, a species that is likely to be diamagnetic by comparison to its isoelectronic relatives $P_3^{Si}Fe–N=NMe$ (vide infra) and $P_3^{Si}Fe–N=NSiMe_3$[16] and as corroborated by DFT calculations that reveal an estimated singlet–triplet gap of 18 kcal/mol for $P_3^{Si}Fe–N=NH$. EPR signatures for the previously characterized $S = 1/2$ $P_3^{Si}Fe=N–NH_2$ and $P_3^{Si}Fe–N_2$ complexes are instead observed (eq 3; Supporting Information).[13b] Similar EPR features are observed when $[P_3^{Si}Fe=N–NH_2][OTf]$ is mixed with NEt_3 at 138 K (eq 3; Supporting Information). To explain these observations, we suggest that a rapid disproportionation of transient $P_3^{Si}Fe–N=NH$ may occur via intermolecular H atom transfer to furnish a 1:1 mixture of $P_3^{Si}Fe–N_2$ and $P_3^{Si}Fe=N–NH_2$ (Scheme 3).[23] For this disproportionation process to proceed, the $BDE_{N–H}$ or $BDFE_{N–H}$ of $P_3^{Si}Fe–N=NH$ must be less than that of $P_3^{Si}Fe=N–NH_2$. We note that $P_3^{Si}Fe=N–NH_2$ is itself highly reactive and can only be prepared in thawing 2-MeTHF (138 K). Collectively, these observations hint at very reactive N–H bonds in $P_3^{Si}Fe–N=NH^{+/0}$ and $P_3^{Si}Fe=N–NH_2^{+/0}$. The magnitude of these values are refined in the following section.

The N–H Bond Enthalpy of the Iron Hydrazido Complex $P_3^{Si}Fe=N–N(Me)H^+$ and Estimates of the N–H Enthalpies of $P_3^{Si}Fe=N–NH_2$ and $P_3^{Si}Fe–N=NH$

To gain more quantitative insight into the reactive N–H bonds of certain protonated $P_3^{Si}Fe–N_xH_y$ species, we examined the reactivity of the quasi-stable methyldiazenido complex, $P_3^{Si}Fe–N=NMe$, and its more stable conjugate acid, $[P_3^{Si}Fe=N–N(Me)H][OTf]$. $P_3^{Si}Fe–N=NMe$ is generated via the reaction of $[K(Et_2O)_n][P_3^{Si}Fe–N_2]$ with MeOTf at 195 K (Scheme 4) and is stable for hours at this temperature but rapidly decays at ambient temperatures ($\tau_{(273k)}$ = 14 min) to a mixture of $[P_3^{Si}Fe=N–NMe_2][OTf]$ and $P_3^{Si}Fe–OTf$. At 193 K, NMR analysis reveals the presence of two distinct structural isomers of diamagnetic $P_3^{Si}Fe–N=NMe$ that give rise to independent sets of multinuclear NMR parameters (refer to the Supporting Information for further discussion and spectra). Nonetheless, sharp resonances in the $^{15}N\{^1H\}$ NMR spectrum at $\delta \approx 471$ and 274 ppm characterize the N atoms of the diazenido ligand; these resonance are distinct from those of $[P_3^{Si}Fe=N–NMe_2][OTf]$ (δ = 530, 185 ppm) and $[K\text{-}(Et_2O)_n][P_3^{Si}Fe–N_2]$ (δ = 340, 310 ppm).[13b,16] The position of the $[P_3^{Si}Fe–N=NMe]$-derived ^{15}N resonances are reasonably similar to those of

the isoelectronic and structurally characterized iron-silyldiazenido, $P_3^{Si}Fe–N=NSiMe_3$ (419 and 271 ppm).[16] In situ IR spectra of THF solutions containing $P_3^{Si}Fe–N=NMe$ and ^{15}N-enriched-$P_3^{Si}Fe–N=NMe$ reveal broad and intense features at 1616 and 1568 cm^{-1}, respectively, that are diagnostic of terminally bound diazenido ligands (Figure 2). These $\nu(N=N)$ values are substantially lower than those of $P_3^{Si}Fe–N=NSiMe_3$ (1748 and 1694 cm^{-1} for the ^{14}N and ^{15}N isotopomers, respectively).[16] These spectroscopic differences indicate a higher degree of N=N bond activation in $P_3^{Si}Fe–N=NMe$ as compared to $P_3^{Si}Fe–N=NSiMe_3$. Accordingly, $P_3^{Si}Fe–N=NMe$ reacts productively with electrophiles (such as Me^+ or H^+, vide infra), whereas $P_3^{Si}Fe–N=NSiMe_3$ does not.

Protonation of $P_3^{Si}Fe–N=NMe$ generated in situ with HOTf at 195 K results in an immediate color change to lavender, and subsequent addition of pentane enables the isolation of $[P_3^{Si}Fe=N–N(Me)H][OTf]$ (Scheme 4) as a crystalline pink powder. NMR data for $[P_3^{Si}Fe=N–N(Me)-H][OTf]$ are similar to those of $[P_3^{Si}Fe=N–NH_2][OTf]$[13b] and include two resonances in the $^{15}N\{^1H\}$ NMR spectrum (δ = 518 and 199 ppm) with the upfield resonance coupled to a single H atom ($^1J_{NH}$ = 101 Hz), an N–*H* resonance at 9.96 ppm in the ^1H NMR spectrum and a single ^{31}P resonance at 97 ppm. Broad features ascribed to N–H vibrations are observed in the solid IR spectrum of $[P_3^{Si}Fe=N–N(Me)H][OTf]$ at =2980 cm^{-1} that shift to ~2295 cm^{-1} in $[P_3^{Si}Fe=N–N(Me)D][OTf]$; the low frequency of these features are suggestive of strong hydrogen bonding interactions in the solid state. The solid-state crystal structure of $[P_3^{Si}Fe=N–N(Me)-H][OTf]$ (Figure 3) corroborates the spectroscopic data and reveals a short Fe–N distance of 1.671(3) Å, a long N–N distance (1.284(4) Å), and a strong hydrogen bond (d(N···O) 2.846(4), ∠(N–H···O) 164(4)°) between the OTf anion and the hydrazido ligand.

Analytical data collected on $P_3^{Si}Fe–N=NMe$ and $[P_3^{Si}Fe=N–N(Me)H][OTf]$ allow for the estimation of the $BDE_{N–H}$ of the latter species. Cyclic voltammetry studies of $P_3^{Si}Fe–N=NMe$ at 195 K in a 50 mM $NaBAr^F{}_{24}$ THF electrolyte reveal a single well-behaved oxidation event centered at −1.22 V versus Fc/Fc^+ (Figure 2). The apparent acidity of $[P_3^{Si}Fe=N–N(Me)H][OTf]$ was determined via its reaction with organic bases at 193 K in THF to regenerate $P_3^{Si}Fe–N=NMe$. While 1.1 equiv of NEt_3 ($pK_{b(THF)}$ = 13.7) quantitatively converts $[P_3^{Si}Fe=N–N(Me)H][OTf]$ to $P_3^{Si}Fe–N=NMe$, the addition of 9.6 equiv of 2-Cl-$PhNH_2$ ($pK_{b(THF)}$ = 6.0) to $[P_3^{Si}Fe=N–N(Me)H][OTf]$ results in little detectable $P_3^{Si}Fe–N=NMe$ (Figure 4A). The addition of $PhNH_2$ ($pK_{b(THF)}$ = 8.0) or 4-Cl-$PhNH_2$ ($pK_{b(THF)}$ = 7.0) to solutions of $[P_3^{Si}Fe=N–N(Me)H][OTf]$ results in immediate deprotonation to afford mixtures of $P_3^{Si}Fe–N=NMe$ and $[P_3^{Si}Fe=N–N(Me)H]$-[OTf] that persist at 193 K for 30 min (Figure 4B,C). Subsequent analysis of the resulting Fe speciation reveals an average pK_a = 8.0(2) for the hydrazido ligand of $[P_3^{Si}Fe=N–N(Me)H][OTf]$ in THF solution. Combined with the oxidation potential for $P_3^{Si}Fe–N=NMe$ (vida supra), the application of eq 1 provides an estimate of $BDE_{N–H}$ = 49(1) kcal/mol for $[P_3^{Si}Fe=N–N(Me)H][OTf]$ (Table 1).

The thermal instability exhibited by the species more mechanistically relevant to N_2-to-NH_3 conversion, $P_3^{Si}Fe=N–NH_2{}^{0/+}$, precludes the collection of similar experimental data. Nonetheless, knowledge of the redox properties of $P_3^{Si}Fe–N=NMe$ (E_{ox} = −1.22 V) and $P_3^{Si}Fe=N–NMe_2$ (E_{ox} = −1.73 V) coupled with the experimental acidity of $P_3^{Si}Fe=N–$

N(Me)H$^+$ (pK_a = 8.0) allow for rough estimations of the N–H bond strengths of $P_3^{Si}Fe{=}N{-}NH_2^{0/+}$. If we plausibly assume that $P_3^{Si}Fe$–N=NMe displays a similar basicity to $P_3^{Si}Fe$–N=NH, then we approximate the BDE_{N-H} for $P_3^{Si}Fe{=}N{-}NH_2^+$ as 49 kcal/mol. Additionally, if we assume that $P_3^{Si}Fe{=}N{-}NMe_2^+$ and $P_3^{Si}Fe{=}N{-}NH_2^+$ are reduced at similar potentials, the BDE_{N-H} of $P_3^{Si}Fe{=}N{-}NH_2$ may be estimated as 37 kcal/mol. DFT-predicted BDE_{N-H} values for these species in the gas-phase are in excellent agreement with these estimations: 35 and 49 kcal/mol are predicted for the neutral and cationic $P_3^{Si}Fe{=}N{-}NH_2$ species, respectively (Supporting Information). In this context, the formation of $P_3^{Si}Fe{=}N{-}NH_2$ (and $P_3^{Si}Fe{-}N_2$) via disproportionation of $P_3^{Si}Fe$–N=NH (Scheme 3) allows us to place a reasonable upper bound on the BDE_{N-H} of $P_3^{Si}Fe{-}N{\equiv}NH$ at 37 kcal/mol. The magnitude of this value speaks to a high degree of N=N bond activation that occurs concomitant with the delivery of the first and second hydrogen atoms.

Thermoneutral H$^+$/e$^-$ Equilibria between $P_3^{Si}Fe{-}C{\equiv}NMe^{0/+}$ and $P_3^{Si}Fe{\equiv}C{-}N(Me)H^{0/+}$

Attempts to determine the BDE_{N-H} of the aminocarbyne $[P_3^{Si}Fe{=}C{-}NH_2][OTf]$ are in part hampered by the tendency of this compound to spontaneously decay with formation of H_2 and NH_3.[12] Moreover, attempts to isolate neutral $P_3^{Si}Fe{=}C{=}NH$ via the reaction of $[P_3^{Si}Fe{-}C{\equiv}NH][BArF_{24}]$ with stoichiometric Cp*$_2$Co result only in intractable mixtures of Fe species, presumably reflecting the low BDE_{N-H} estimated for $P_3^{Si}Fe{=}C{=}NH$ (44 kcal/mol). We therefore examined the reactivity of the isoelectronic alkylisocyanide complex, $P_3^{Si}Fe{=}C{=}NMe$ (Scheme 5). This complex facilitates access to an iron-aminocarbyne-derived N–H bond suitable for analytical study and provides calibration for the BDE_{N-H} of $P_3^{Si}Fe{\equiv}C{-}NH_2^+$, the latter species (presumably) being a mechanistically relevant early stage intermediate in Fe–mediated CN^- reduction to NH_3 and CH_4.[12]

In contrast to $P_3^{Si}Fe{=}C{=}NH$, both neutral $P_3^{Si}Fe{=}C{=}NMe$ and one-electron oxidized $[P_3^{Si}Fe{-}C{\equiv}NMe][OTf]$ are stable in the solid state (Figure 3) and as THF solutions at room temperature. The cyclic voltammogram of a THF electrolyte solution of $P_3^{Si}Fe{=}C{=}NMe$ displays a one-electron oxidation event at −1.31 V (Figure 5). Exposure of $P_3^{Si}Fe{=}C{=}NMe$ to 1 equiv of $[H(OEt_2)_2][BArF_{24}]$ in Et_2O and subsequent workup furnishes the secondary aminocarbyne complex, $[P_3^{Si}Fe{\equiv}C{-}N(Me)H][BArF_{24}]$, as a purple solid that slowly converts to $[P_3^{Si}Fe{-}C{\equiv}NMe][BArF_{24}]$ overnight in room temperature THF solution with the concomitant loss of H_2 (0.4 equiv/Fe measured by GC; eq 3).

$$[P_3{}^{Si}Fe \equiv C{-}N(H)Me][BAr^F{}_{24}] \rightarrow [P_3{}^{Si}Fe{-}C \equiv NMe][BAr^F{}_{24}] + {}^1\!/_2\, H_2 \quad (3)$$

$P_3^{Si}Fe{=}C{=}NMe$ and $[P_3^{Si}Fe{=}C{-}N(Me)H][BArF_{24}]$ are distinct by EPR ($P_3^{Si}Fe{=}C{=}NMe$, g_1 = 2.37, g_2 = 2.02; $[P_3^{Si}Fe{\equiv}C{-}N(Me)H][BArF_{24}]$, g_1 = 2.54, g_2 = 1.97) and ^{57}Fe Mossbauer spectroscopy ($P_3^{Si}Fe{=}C{=}NMe$, δ = 0.25, ΔE_Q = 1.47; $[P_3^{Si}Fe{\equiv}C{-}N(Me)H][BArF_{24}]$, δ = 0.16, ΔE_Q = 1.51) (Figure 5). $[P_3^{Si}Fe{\equiv}C{-}N(Me)H][BArF_{24}]$ additionally displays a sharp feature at 3337 cm^{-1} in its solid-state IR spectrum that shifts to 2478 cm^{-1} in $[P_3^{Si}Fe{\equiv}C{-}N(Me)D][BArF_{24}]$, assigned as the N–H and N-D stretching frequencies, respectively. The solid-state crystal structure (Figure 3) of $[P_3^{Si}Fe{\equiv}C{-}N(Me)H][BArF_{24}]$ reveals a short Fe–C

bond (1.751(9) Å) and a long C–N bond (1.28(1) Å) relative to those of $P_3^{Si}Fe{=}C{=}NMe$ (d(*Fe*–C), 1.821(2) Å, d(C–N), 1.186(2) Å), consistent with a terminally bound aminocarbyne ligand (Table 2).[24] The cyclic voltammogram of freshly prepared $[P_3^{Si}Fe{=}C{-}N(Me)H][BAr^F{}_{24}]$ in THF displays a reversible one-electron reduction event at −1.27 V (Figure 5, Table 1). $[P_3^{Si}Fe{=}C{-}N(Me)H]$ $[BAr^F{}_{24}]$ is quantitatively deprotonated upon exposure to 1.1 equiv of NEt_3 in THF solution, reforming $P_3^{Si}Fe{=}C{=}NMe$ and establishing reversible proton transfer under these conditions.

Unlike the titration experiments performed with $P_3^{Si}Fe{-}CN$ and $P_3^{Si}Fe{=}N{-}N(Me)H^+$, the reaction of $P_3^{Si}Fe{=}C{=}NMe$ with substoichiometric proton equivalents is complicated by competing electron or H atom transfer processes (Figure 6A–C). While the exposure of $P_3^{Si}Fe{=}C{=}NMe$ to 4 equiv of [2-Cl-PhNH$_3$][OTf] results in the quantitative formation of $[P_3^{Si}Fe{\equiv}C{-}N(Me)H][OTf]$; features assigned to those of the one-electron oxidized iron isocyanide complex, $[P_3^{Si}Fe{-}C{\equiv}NMe][OTf]$, and the neutral iron aminocarbyne $P_3^{Si}Fe{\equiv}C{-}N(Me)H$ (vide infra) are observed at earlier stages of the titration (Figure 6A,B). On further addition of proton equivalents, the expected features of $[P_3^{Si}Fe{\equiv}C{-}N(Me)H]$-[OTf] grow in with the concomitant loss of features assigned to the neutral $P_3^{Si}Fe{\equiv}C{-}N(Me)H$ and $[P_3^{Si}Fe{-}C{=}NMe]$-[OTf] (Figure 6C). This series of spectral changes has been observed with a variety of chlorinated anilinium salts and with subsubstoichiometric amounts of $[H(OEt_2)2][BAr^F{}_{24}]$. Inspection of the available cyclic voltammetry data (Figure 5A) indicates that the *oxidation* of $P_3^{Si}Fe{=}C{=}NMe$ occurs at nearly the same potential as the reduction of $[P_3^{Si}Fe{\equiv}C{-}N(Me)H][BAr^F{}_{24}]$. Solutions generated during the acid titration experiments contain mixtures of these two species and are hence prone to spontaneously disproportionate to an equilibrium mixture of $P_3^{Si}Fe{-}CNMe^{+/0}$ and $P_3^{Si}Fe{=}C{-}N(Me)H^{+/0}$ (illustrated schematically in Figure 6D).

Multinuclear NMR spectroscopy was employed to provide direct evidence for the competing H^+/e^- transfer processes observed in solutions containing both $P_3^{Si}Fe{=}C{=}NMe$ and $P_3^{Si}Fe{\equiv}C{-}N(Me)H^+$. The presented model (Figure 6D) predicts the accumulation of neutral and diamagnetic $P_3^{Si}Fe{\equiv}C{-}N(Me)H$ via an intermolecular electron or H atom transfer between $P_3^{Si}Fe{=}C{=}NMe$ and $P_3^{Si}Fe{=}C{-}N(Me)H^+$. To mimic the conditions at the midpoint of an acidity titration, $P_3^{Si}Fe{=}{}^{13}C{=}NMe$, $P_3^{Si}Fe{=}C{=}{}^{15}NMe$, and $[H(OEt_2)_2]$-$[BAr^F{}_{24}]$ can be dissolved in THF-d_8 in a 1:1:1 ratio at 193 K, and the resulting solution can be analyzed by multinuclear NMR spectroscopy. At this temperature, a sharp doublet ($^1J_{NH}$ 93 Hz) in the ^{15}N NMR spectrum appears at δ = 135.2 ppm that is attributed to diamagnetic $P_3^{Si}Fe{\equiv}C{-}N(Me)H$.[25] The chemical shift of this resonance is comparable to that of structurally characterized and isoelectronic $P_3^{Si}Fe{\equiv}C{-}NMe_2$ (129.1 ppm), and the magnitude of $^1J_{NH}$ unambiguously confirms the presence of an N–H unit.[12] Two resonances are observed in the $^{13}C\{^1H\}$ NMR spectrum at δ = 279.7 and 282.7 ppm that may be assigned to aminocarbyne carbons of two slightly different structural isomers of $P_3^{Si}Fe{\equiv}C{-}N(Me)H$.[26] These NMR data confirm the spontaneous generation of $P_3^{Si}Fe{\equiv}C{-}N(Me)H$ in these solutions despite the absence of an exogenous reductant or H atom source and support the hypothesis that $P_3^{Si}Fe{=}C{=}NMe$ and $P_3^{Si}Fe{=}C{-}N(Me)H^{(+)}$ are subject to rapid, reversible, and nearly thermoneutral H^+/e^- transfer in THF solutions at temperatures as low as 193 K.

Despite the complex speciation resulting from acid titrations of $P_3^{Si}Fe{\equiv}C{=}NMe$, the p$K_a$ for $P_3^{Si}Fe{\equiv}C{-}N(Me)H^{(+)}$ can be determined by the deconvolution of the spectral data at a known acid concentration to define the relative proportions of the individual Fe species (see the Supporting Information for details). A pure spectrum of neutral $P_3^{Si}Fe{\equiv}C{-}N(Me)H$ is unavailable, however, as attempts to isolate this compound in pure form have been unsuccessful ($\tau_{(1/2)} < 60$ min in THF at 273 K). Available NMR data indicates that neutral $P_3^{Si}Fe{\equiv}C{-}NMe_2$ expectedly bears a similar electronic structure to $P_3^{Si}Fe{\equiv}C{-}N(Me)H$, hence providing a model UV–visible absorption spectrum of the latter species.[27] Indeed, the spectra shown in Figure 6 are satisfactorily simulated by a linear combination of the pure spectra of $[P_3^{Si}Fe{-}C{\equiv}NMe][OTf]$, $[P_3^{Si}Fe{\equiv}CN(Me)H][OTf]$, $P_3^{Si}Fe{=}C{=}NMe$, and $P_3^{Si}Fe{\equiv}C{-}NMe_2$ (as a surrogate for $P_3^{Si}Fe{\equiv}C{-}N(Me)H$). Analysis of the spectral data obtained by titrating $P_3^{Si}Fe{=}C{=}NMe$ with $[PhNH_3][OTf]$ (pK_a = 8.0), [4-Cl-$PhNH_3$][OTf] (pK_a = 7.0), and [2-Cl-$PhNH_3$][OTf] (pK_a = 6.0) reveals an average pK_a of 7.1(3) for the acidic proton of $[P_3^{Si}Fe{=}C{-}N(Me)H][OTf]$ in THF. Using this value, the relevant BDE_{N-H} values for $[P_3^{Si}Fe{\equiv}C{-}N(Me)H][OTf]$ and $P_3^{Si}Fe{\equiv}C{-}N(Me)H$ are estimated with eqs 1 and 2 and found to be 47(1) and 46(1) kcal/mol, respectively, corroborating the plausibility of intermolecular H atom transfer between $P_3^{Si}Fe{=}C{=}NMe$ and $[P_3^{Si}Fe{\equiv}C{-}N(Me)H][OTf]$ in solution (Table 1, Figure 6).

The invariance of the BDE_{N-H} within the $P_3^{Si}Fe{\equiv}C{-}N(Me)H^{+/0}$ redox series is unusual and starkly contrasts that of the $P_3^{Si}Fe{-}CNH^{+/0}$ redox series. In general, the one-electron oxidation of transition metal complexes that bear X–H (X = N, O) bonds results in a noted increase in BDE_{X-H}.[15d,28] The BDE_{M-H} values measured in redox-active metal hydride species also display significant oxidation state dependence, but in this case the trend is reversed.[29] The equivalent BDE_{N-H} values observed for $P_3^{Si}Fe{\equiv}C{-}N(Me)H$ underscores their similar hybridizations at N(sp) and also likely reflects similar degrees of C–N bond weakening upon H atom addition to $P_3^{Si}Fe{-}CNMe^{+/0}$. Strong backbonding from Fe to C in the isocyanide $P_3^{Si}Fe{=}C{=}NMe$ causes bending at N, favoring a resonance contributor with significant Fe to C π-bonding (as opposed to $P_3^{Si}Fe{-}C{\equiv}NMe$). This is born out in its crystal structure (Figure 3) and may serve to minimize structural reorganization associated with H atom transfer between $P_3^{Si}Fe{=}C{=}NMe$ and $[P_3^{Si}Fe{=}C{-}N(Me)H][OTf]$. Collectively, these facile H atom transfer reactions provide a model for the various disproportionation reactions invoked for the $P_3^{Si}Fe{-}N{=}NH^{0/+}$ and $P_3^{Si}Fe{=}N{-}NH_2^{0/+}$ species discussed above.

Concluding Remarks

The N_2-to-NH_3 conversion mediated by biological and synthetic systems requires the delivery of multiple proton/ electron equivalents to N_2 via various intermediates. We have speculated that $P_3^{X}Fe$–based catalysts are likely to operate via mechanisms that initiate along a “distal” pathway, and previous studies indicate similar mechanisms for a conceptually related stoichiometric conversion of CN^- to CH_4 and NH_3 by the $P_3^{Si}Fe$ system. Synthetic access to rare examples of Fe–N=NR, Fe=N–NR_2, Fe–CNR, and Fe=C–NR_2 species (R = H, Me) derived from $P_3^{Si}Fe{-}N_2$/CN has enabled the in-depth study of relevant intermediates in these proposed mechanisms. The measurements of pertinent redox and acidity values for many of these species reported herein indicate that that these early intermediates display weak N–H bonds, ranging from <37 to 65 kcal/mol. This range of

values is likely to be linked to the varying degrees of N≡N or C≡N bond weakening that occurs concomitant with H atom addition.

A noteworthy exception to the preceding manifold ofcharacterized compounds is the initial intermediate of N_2-to-NH_3 conversion, $P_3^{Si}Fe–N=NH^{+/0}$, which has eluded directspectroscopic detection. $P_3^{Si}Fe–N=NH^+$ is apparently tooacidic to observe in ethereal solvents and neutral $P_3^{Si}Fe–N=NH$ appears to undergo rapid disproportionation to $P_3^{Si}Fe=N–NH_2$ and $P_3^{Si}Fe–N_2$ at temperatures as low as 138 K.Experimentally, we can assign an upper limit of 37 kcal/mol forthe $BDE_{N–H}$ of $P_3^{Si}Fe–N=NH$ by comparison toappropriate model complexes. This suggests that the initial Hatom addition to $P_3^{Si}Fe–N_2$ is likely the most thermody-namically uphill step in the overall N_2-to-NH_3 conversion.Theoretical studies suggests that this step is also challenging inthe biological system[8b,30] and highlight the possibility of cooperative activation of N_2 by two or more of the metal ions in the active-site cofactor. Indeed, numerous bimetallic complexes have been shown to stabilize diazenido and diazene ligands, [6d,31] and the stability of these complexes may be ascribed to cooperative N=N bond activation by the two metal centers. These considerations certainly motivate further development of multimetallic platforms capable of reductive N_2 protonation.

The reactions of the various protonated $P_3^{Si}Fe–N_2$/CN species studied herein have been conducted in relative isolation under well-defined conditions. While these individual reactions are likely mechanistically relevant to catalytic and stoichiometric N_2/CN^- reductions, these conditions contrast those employed in catalytic NH_3 synthesis, namely, the *simultaneous* inclusion of excess inorganic acid and reductant sources in Et_2O. Under these conditions, both H_2 evolution and N–H bond formation reactions will proceed at unique rates that will depend on the choice of Fe precatalysts and the nature of these reagents and will hence compete for the H^+/e^- equivalents present in solution. Both of these processes are undoubtedly facilitated by the low BDE_{NH} values exhibited by these species, but these thermodynamic values are only indirectly linked to the rates of the relevant N–H bond formation and N–N or C– N cleavage reactions. Detailed kinetic investigations of these processes should shed light on additional factors that govern proton-coupled N_2 fixation by molecular Fe systems. The complexes described herein will provide useful synthons for such investigations.

Supplementary Material

Refer to Web version on PubMed Central for supplementary material.

Acknowledgments

This work was supported by the NIH (Grant GM 070757) and the Gordon and Betty Moore Foundation. J.R. was additionally supported by a fellowship from the Caltech Center for Environmental Microbial Interactions (CEMI).

References

1. Schlögl R. Angew Chem, Int Ed. 2003; 42:2004–2008.
2. (a) Brown KA, Harris DF, Wilker MB, Rasmussen A, Khadka N, Hamby H, Keable S, Dukovic G, Peters JW, Seefeldt LC, King PW. Science. 2016; 352:448–450. [PubMed: 27102481] (b) Liu J,

Kelley MS, Wu W, Banerjee A, Douvalis AP, Wu J, Zhang Y, Schatz GC, Kanatzidis MG. Proc Natl Acad Sci U S A. 2016; 113:5530–5535. [PubMed: 27140630] (c) Lehnert N, Peters JC. Inorg Chem. 2015; 54:9229–9223. [PubMed: 26434648] (d) Michalsky R, Pfromm PH, Steinfeld A. Interface Focus. 2015; 5:20140084. [PubMed: 26052421]

3. Jia HP, Quadrelli EA. Chem Soc Rev. 2014; 43:547–564. [PubMed: 24108246]
4. (a) Kuriyama S, Arashiba A, Nakajima K, Matsuo Y, Tanaka H, Ishii K, Yoshizawa K, Nishibayashi T. Nat Commun. 2016; 7:12181. [PubMed: 27435503] (b) Hill PJ, Doyle LR, Crawford AD, Myers WK, Ashley AE. J Am Chem Soc. 2016; 138:13521–13524. [PubMed: 27700079] (c) Yandulov DV, Schrock RR. Science. 2003; 301:76–78. [PubMed: 12843387] (d) Ritleng V, Yandulov DV, Weare WW, Schrock RR, Hock AS, Davis WM. J Am Chem Soc. 2004; 126:6150–6163. [PubMed: 15137780] (e) Arashiba K, Kinoshita E, Kuriyama S, Eizawa A, Nakajima K, Tanaka H, Yoshizawa K, Nishibayashi Y. J Am Chem Soc. 2015; 137:5666–5669. [PubMed: 25879994] (f) Kuriyama S, Arashiba K, Tanaka H, Matsuo Y, Nakajima K, Yoshizawa K, Nishibayashi Y. Angew Chem, Int Ed. 2016; 55:14291–14295.
5. (a) Howard JB, Rees DC. Chem Rev. 1996; 96:2965–2982. [PubMed: 11848848] (b) Seefeldt LC, Hoffman BM, Dean DR. Annu Rev Biochem. 2009; 78:701–722. [PubMed: 19489731] (c) Burgess BK, Lowe DJ. Chem Rev. 1996; 96:2983–2011. [PubMed: 11848849]
6. Representative examples include Chatt J, Pearman AJ, Richards RL. J Chem Soc, Dalton Trans. 1977:1852–1860.Laplaza CE, Cummins CC. Science. 1995; 268:861–863. [PubMed: 17792182] Shima T, Hu SW, Luo G, Kang XH, Luo Y, Hou ZM. Science. 2013; 340:1549–1552. [PubMed: 23812710] Fryzuk MD, Love JB, Rettig SJ, Young VG. Science. 1997; 275:1445–1447.
7. (a) Yandulov DV, Schrock RR. J Am Chem Soc. 2002; 124:6252–6253. [PubMed: 12033849] (b) Yandulov DV, Schrock RR. Inorg Chem. 2005; 44:1103–1117. [PubMed: 15859292] (c) Weare WW, Dai X, Byrnes MJ, Chin JM, Schrock RR, Muller P. Proc Natl Acad Sci U S A. 2006; 103:17099–17106. [PubMed: 17085586] (d) Munisamy T, Schrock RR. Dalton Trans. 2012; 41:130–137. [PubMed: 22031021] (e) Chatt J, Dilworth J, Richards RL. Chem Rev. 1978; 78:589–625.
8. (a) Spatzal T, Perez KA, Einsle O, Howard JB, Rees DC. Science. 2014; 345:1620–1623. [PubMed: 25258081] (b) Lukoyanov D, Khadka N, Yang ZY, Dean DR, Seefeldt LC, Hoffman BM. J Am Chem Soc. 2016; 138:10674. [PubMed: 27529724] (c) Hinnemann B, Norskov JK. Top Catal. 2006; 37:55–70.(d) Schneider K, Gollan E, Dröttboom M, Selsemeier-Voigt S, Müller A. Eur J Biochem. 1997; 244:789–800. [PubMed: 9108249]
9. (a) Rodriguez MM, Bill E, Brennessel WW, Holland PL. Science. 2011; 334:780–783. [PubMed: 22076372] (b) Macleod KC, McWilliams SF, Mercado BQ, Holland PL. Chem Sci. 2016; 7:5736–5746. [PubMed: 28066537]
10. Lee Y, Sloane FT, Blondin G, Abboud KA, Garcia-Serres R, Murray LJ. Angew Chem, Int Ed. 2015; 54:1499–1503.
11. (a) Anderson JS, Rittle J, Peters JC. Nature. 2013; 501:84–87. [PubMed: 24005414] (b) Creutz SE, Peters JC. J Am Chem Soc. 2014; 136:1105–1115. [PubMed: 24350667] (c) Ung G, Peters JC. Angew Chem, Int Ed. 2015; 54:532–535.(d) Del Castillo TJ, Thompson NB, Peters JC. J Am Chem Soc. 2016; 138:5341–5350. [PubMed: 27026402]
12. Rittle J, Peters JC. Angew Chem, Int Ed. 2016; 55:12262–12265.
13. (a) Anderson JS, Cutsail GE, Rittle J, Connor BA, Gunderson WA, Zhang LM, Hoffman BM, Peters JC. J Am Chem Soc. 2015; 137:7803–7809. [PubMed: 26000443] (b) Rittle J, Peters JC. J Am Chem Soc. 2016; 138:4243–4248. [PubMed: 26937584]
14. The Lewis structures we adopt provide simple representations that emphasize aspects of the bonding but are not reliable representations as such. For example, we draw $P_3^{Si}Fe(CNH)^{+/0}$ as $P_3^{Si}Fe–C{\equiv}NH^{+}$ or $P_3^{Si}Fe{=}C{=}NH^{0}$, and these representations are informed by available structural, spectroscopic, or theoretical data. Additionally we draw $P_3^{Si}Fe(NNH)$ as $P_3^{Si}Fe–N{=}NH$ but realize that in all cases there is varying degrees of $\boldsymbol{\pi}$-bonding between Fe and the connected C- or N-atom.
15. (a) Bezdek MJ, Chirik PJ. Dalton Trans. 2016; 45:15922–15930. [PubMed: 27378665] (b) Pappas I, Chirik PJ. J Am Chem Soc. 2015; 137:3498–3501. [PubMed: 25719966] (c) Pappas I, Chirik PJ. J Am Chem Soc. 2016; 138:13379–13389.(d) Bezdek MJ, Guo S, Chirik PJ. Science. 2016; 354:730–733. [PubMed: 27846601]

16. Lee Y, Mankad NP, Peters JC. Nat Chem. 2010; 2:558–565. [PubMed: 20571574]
17. Warren JJ, Tronic TA, Mayer JM. Chem Rev. 2010; 110:6961–7001. [PubMed: 20925411]
18. Luo, YR. Comprehensive Handbook of Chemical Bond Energies. CRC Press; Boca Raton: 2007.
19. The estimation of $BDFE_{NH}$ values by this approach is not currently possible in THF as the corresponding C_G value is unavailable. We therefore report BDE_{NH} values, for which a C_H constant in THF is known.[20] While entropic effects may influence these estimated BDE_{NH} values, the general trends shown for these complexes are unlikely to be significantly affected.
20. Cappellani EP, Drouin SD, Jia G, Maltby PA, Morris RH, Schweitzer CT. J Am Chem Soc. 1994; 116:3375–3388.
21. Garrido G, Roses M, Rafols C, Bosch E. J Solution Chem. 2008; 37:689–700.
22. Ding FZ, Smith JM, Wang HB. J Org Chem. 2009; 74:2679–2691. [PubMed: 19275192]
23. The reduction potential of $P_3^{Si}Fe{=}N{-}NH_2^+$ is unknown but is likely similar to that measured for $P_3^{Si}Fe{=}N{-}NMe_2^+$ (−1.7 V), and thus outer sphere electron transfer from $P_3^{Si}Fe{-}N_2^-$ (E_{ox} = −2.1 V) to $P_3^{Si}Fe{=}N{-}NH_2^+$ is an alternative mechanism by which $P_3^{Si}Fe{=}N{-}NH_2$ and $P_3^{Si}Fe{-}N_2$ are generated in these reaction mixtures.
24. The aminocarbyne ligand is disordered over two well-defined positions, but in both instances, a short Fe–C bond (1.751(9) Å and 1.72(2) Å) and long C–N bond (1.28(1) Å and 1.27(2) Å) corroborate the aminocarbyne assignment.
25. Apparently, chemical exchange of the various $P_3^{Si}Fe$ species is slow at this temperature, relative to the NMR time scale. Experiments performed at higher temperatures are complicated by the thermal decomposition of $P_3^{Si}Fe{\equiv}C{-}N(Me)H$.
26. The presence of two resonances likely arises from slightly different geometric isomers of $P_3^{Si}Fe{\equiv}C{-}N(Me)H$ that are trapped out at low temperatures. Indeed, $P_3^{Si}Fe{\equiv}CN{-}Me_2$ similarly displays two features in its $^{13}C\{^1H\}$ NMR spectrum at this temperature (δ = 280.8 and 277.2 ppm), but only one feature is observed at 293 K (δ = 279.1 ppm).[12]
27. Rittle J, Younker JM, Green MT. Inorg Chem. 2010; 49:3610–3617. [PubMed: 20380463]
28. Taguchi T, Stone KL, Gupta R, Kaiser-Lassalle B, Yano J, Hendrich MP, Borovik AS. Chem Sci. 2014; 5:3064–3071. [PubMed: 25580212]
29. Hu Y, Shaw AP, Estes DP, Norton JR. Chem Rev. 2016; 116:8427–8462. [PubMed: 26828562]
30. Dance I. Dalton Trans. 2008:5977–5991. [PubMed: 19082054]
31. (a) Saouma CT, Muller P, Peters JC. J Am Chem Soc. 2009; 131:10358–10359. [PubMed: 19722612] (b) Hirotsu M, Fontaine PP, Zavalij PY, Sita LR. J Am Chem Soc. 2007; 129:12690–12692. [PubMed: 17902670] (c) Pool JA, Lobkovsky E, Chirik PJ. Nature. 2004; 427:527–530. [PubMed: 14765191]

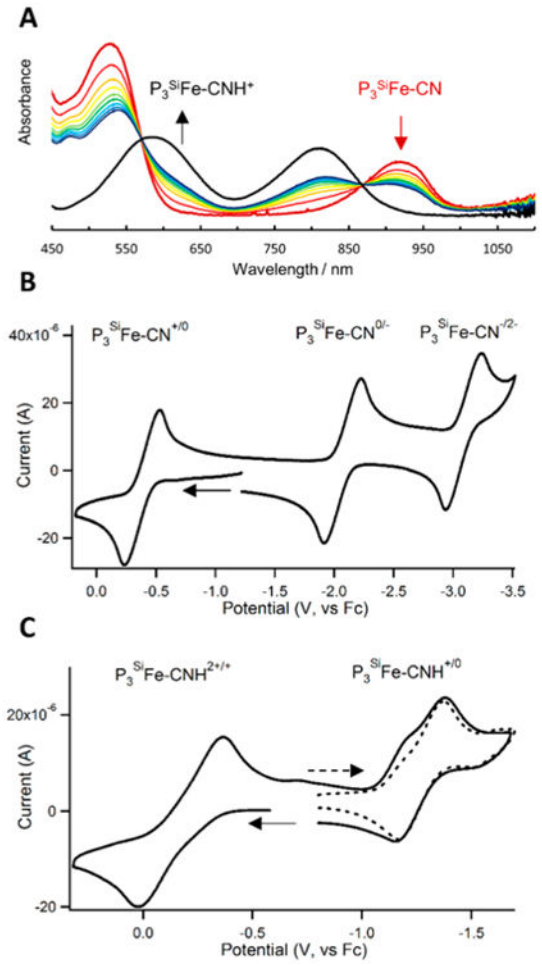

Figure 1.

(A) UV–visible absorption spectra of $P_3^{Si}Fe–CN$ (dark red) and $[P_3^{Si}Fe–C{\equiv}NH][OTf]$ (black) in THF at 25 °C. The other traces were obtained following the sequential addition of 0.33 mol equiv of [2-Cl-$PhNH_3$][OTf] to $P_3^{Si}Fe–CN$. The dark blue trace was obtained following the combined addition of 2.66 equiv [2-Cl-$PhNH_3$][OTf] to $P_3^{Si}Fe–CN$. Arrows indicate features whose intensity increases or decreases during the experiment. Cyclic voltammograms of (B) $P_3^{Si}Fe–CN$ and (C) $[P_3^{Si}Fe–C{=}NH]$-$[BAr^F{}_{24}]$ scanned at 200 mV/s in 0.1 M [TBA][PF_6] THF electrolytes. Solid lines indicate voltammograms initially scanned in the anodic direction, and dashed lines indicate voltammograms initially scanned in the cathodic direction.

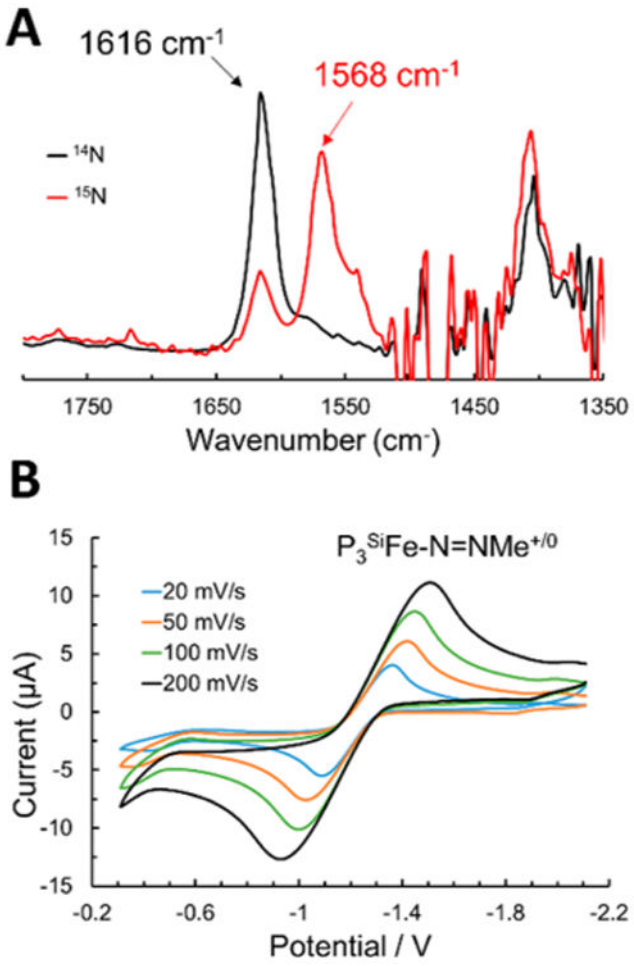

Figure 2.

(A) Overlaid solution IR spectra of THF solutions of in situ-generated $P_3^{Si}Fe–N=NMe$ (black) and N-enriched $P_3^{Si}Fe–N=NMe$ (red) collected at 193 K. (B) Cyclic voltammograms obtained on a 195 K THF solution of $P_3^{Si}Fe–N=NMe$ at the listed scan rate (0.1 M $NaBAr^F_{24}$ electrolyte).

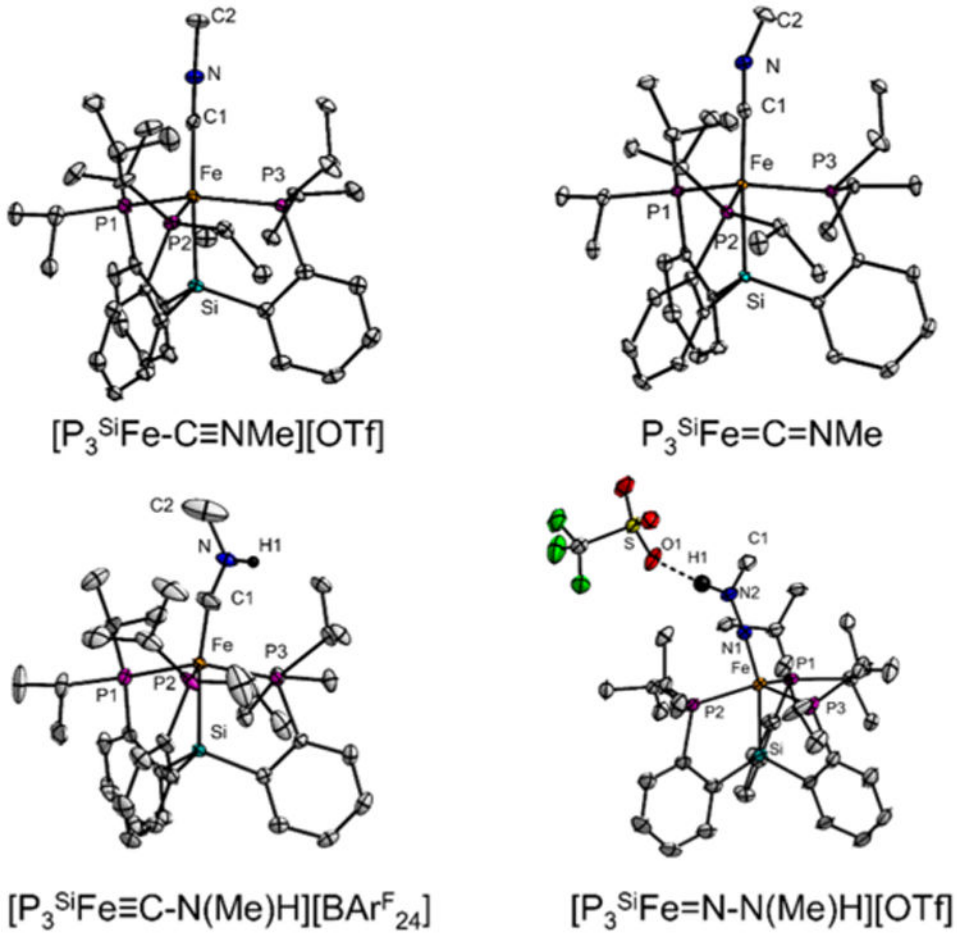

Figure 3.

X-ray diffraction crystal structures of [P_3^{Si}Fe–C≡NMe]-[OTf], P_3^{Si}Fe=C=NMe, [P_3^{Si}Fe=C–N(Me)H][$BAr^F{}_{24}$], and [P_3^{Si}Fe=N–N(Me)H][OTf] with thermal ellipsoids drawn at 50% probability. Hydrogen atoms (except the N–H's), the $BAr^F{}_{24}$ counteranion of [P_3^{Si}Fe=C–N(Me)H][$BAr^F{}_{24}$], and the OTf counteranion of [P_3^{Si}Fe–CNMe][OTf] have been removed for clarity.

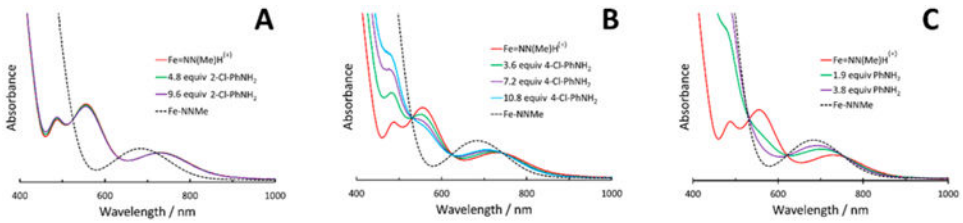

Figure 4.

UV/visible spectra (THF, 198 K) of [P_3^{Si}Fe=N–N(Me)H][OTf] titrated with the listed quantities of (A) 2-Cl-$PhNH_2$, (B) 4-Cl-$PhNH_2$, and (C) $PhNH_2$. Spectra of P_3^{Si}Fe–N=NMe generated with stoichiometric NEt_3 are included for comparison.

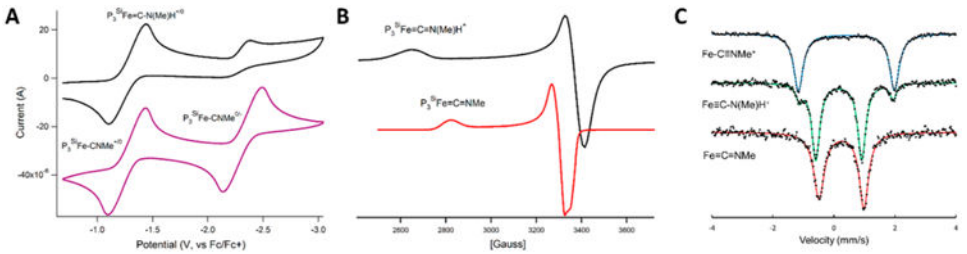

Figure 5.

(A) Cyclic voltammograms obtained on 1 mM solutions of $[P_3^{Si}Fe{\equiv}C{-}N(Me)H][BAr^F24]$ (top) and $P_3^{Si}Fe{=}C{=}NMe$ (bottom) in THF electrolyte (0.1 M [TBA][PF_6]). The traces were obtained at a scan rate of 100 mV/s. (B) EPR spectra of $[P_3^{Si}Fe{=}C{-}N(Me)H][BAr\ 24]$ (black) and $P_3^{Si}Fe{=}C{=}NMe$ (red) recorded at 20 K as 5 mM solutions in 2-Me-THF glass. (C) Zero field ^{57}Fe Mossbauer spectra of $[P_3^{Si}Fe{-}C{\equiv}NMe][OTf]$ (top), $[P_3^{Si}Fe{\equiv}C{-}N(Me)H][BAr^F24]$ (middle), and $P_3^{Si}Fe{=}C{=}NMe$ (bottom) collected at 80 K. The broad signals observed for $P_3^{Si}Fe{=}C{=}NMe$ are attributed to the onset of slow magnetic relaxation. Spectra obtained at 4.2 K can be found in the Supporting Information file.

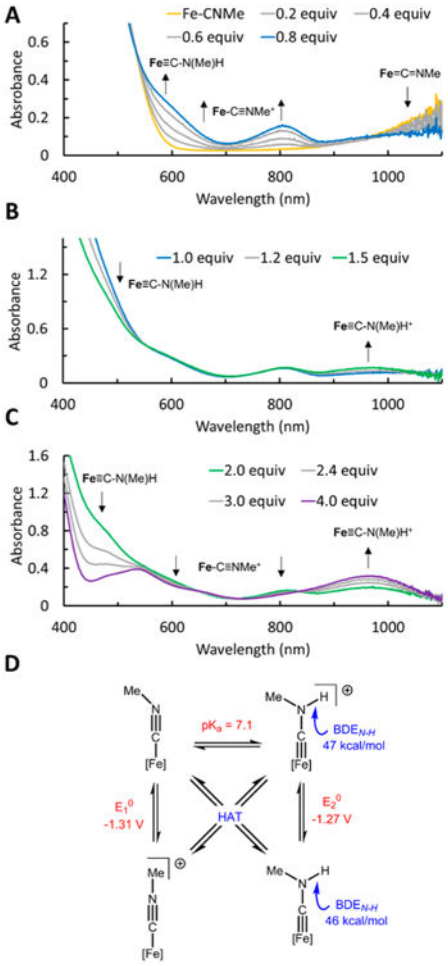

Figure 6.

UV–visible absorption spectra from a representative titration experiment with $P_3^{Si}Fe{=}C{=}NMe$. Spectra shown were obtained following the sequential addition of the listed equivalents of [2-Cl-$PhNH_3$][OTf] to a THF solution of $P_3^{Si}Fe{-}C{\equiv}NMe$ at 298 K. Distinct phases of this addition are shown chronologically in tiles A, B, and C, respectively. Arrows indicate features that increase or decrease during this experiment. (D) Thermochemical data and relevant transformations operative during titration experiments of $P_3^{Si}Fe{=}C{=}NMe$.

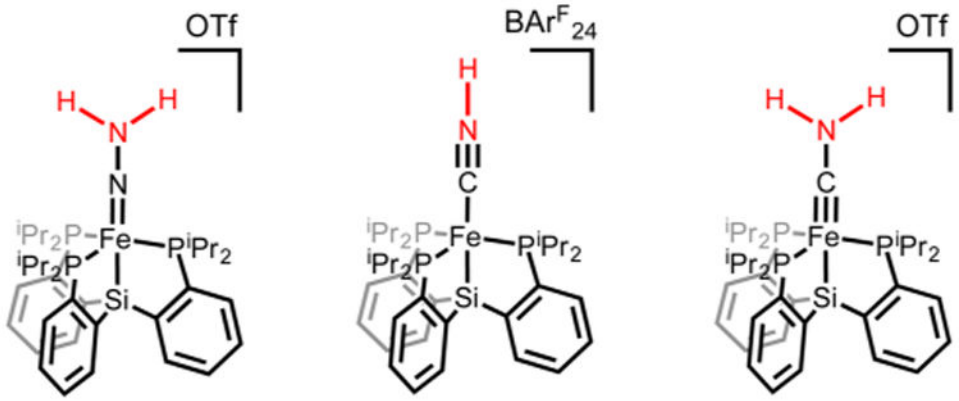

Scheme 1. Previously Reported and Crystallographically Characterized Fe Complexes Derived from Protonation of $P_3^{Si}Fe–N_2$ or $P_3^{Si}Fe$-CN Precursors[12,13b]

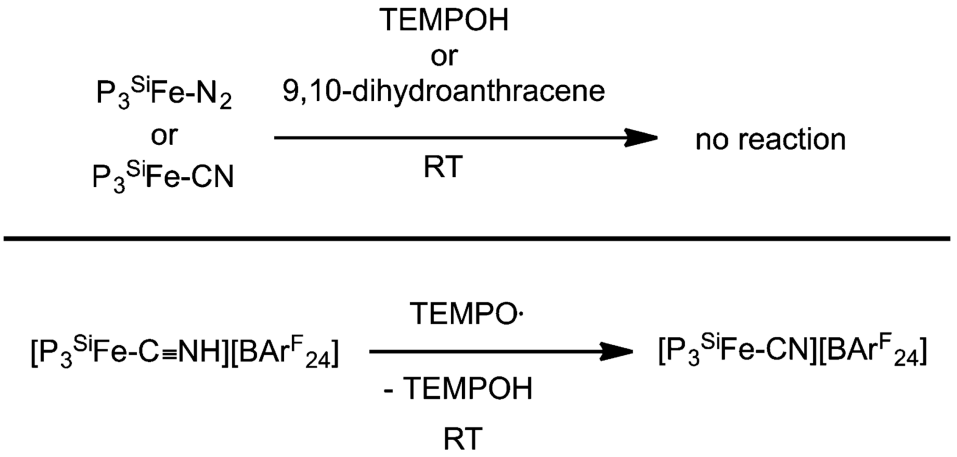

Scheme 2. Hydrogen Atom Transfer Reactions Studied with $P_3^{Si}Fe–N_2$ and $P_3^{Si}Fe$-CN-Derived Compounds

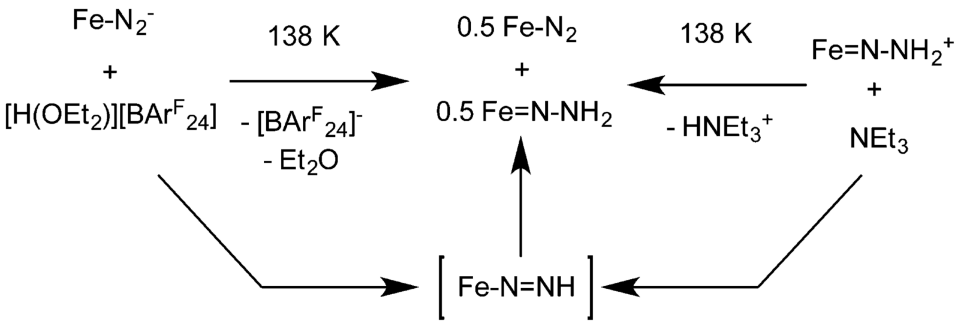

Scheme 3. Suggested Generation and Disproportionation of $P_3^{Si}Fe–N=NH$ to $P_3^{Si}Fe–N_2$ and $P_3^{Si}Fe=N–NH_2$

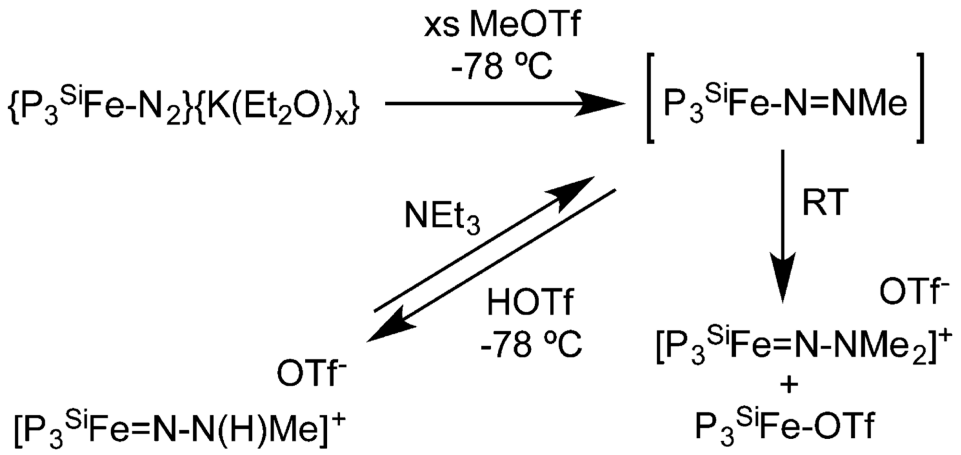

Scheme 4. Synthesis and Interconversion of $P_3^{Si}Fe–N=NMe$ and $[P_3^{Si}Fe=N–N(Me)H][OTf]$

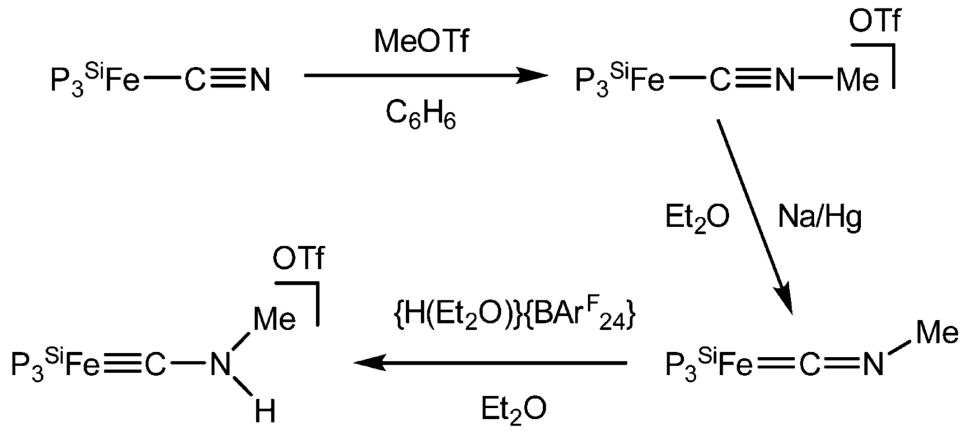

Scheme 5. Synthesis of $P_3^{Si}Fe{=}C{=}NMe$ and $P_3^{Si}Fe{\equiv}C\text{-}N(Me)H$ Complexes[a]

[a]One possible resonance structure for each molecule is shown for clarity.

Table 1
Experimentally Determined Thermodynamic Quantities

compound	pK_a[a]	E_{ox}[b]	$BDE_{N–H}$[c]
$P_3^{Si}Fe–CN$	*d*	−0.38	*d*
$P_3^{Si}Fe–C{\equiv}NH^+$	5.6	−0.17	65
$P_3^{Si}Fe=C=NH$	19[e]	−1.27	44
$P_3^{Si}Fe=C=NMe$	*d*	−1.31	*d*
$P_3^{Si}Fe{\equiv}C–N(Me)H^+$	7.1	*f*	47
$P_3^{Si}Fe{\equiv}C–N(Me)H$	24[e]	−1.27	46
$P_3^{Si}Fe–N{\equiv}N^+$	*d*	−1.1	*d*
$P_3^{Si}Fe–N=NH^+$	≤0	*f*	≤43
$P_3^{Si}Fe–N=NMe$	*d*	−1.22	*d*
$P_3^{Si}Fe=N–N(Me)H^+$	8.0	*f*	48

[a] Acidity values determined in THF.

[b] Redox potentials obtained in THF vs Fc/Fc^+.

[c] Values estimated using eq 1 and 2.

[d] Not relevant.

[e] Values estimated via the application of Hess's law.

[f] Not determined.

Table 2

Relevant Metrical Data[a]

compound	*d*[Fe–C/N][b]	*d*[(C/N)–N][b]	∠[Fe–(C/N)–N][c]	∠[(C/N)–N–(C/H)][c]
$P_3^{Si}Fe–CN^+$	2.025(2)	1.130(3)	179.3(2)	*d*
$P_3^{Si}Fe–CN$	1.973(1)	1.167(1)	179.7(1)	*d*
$P_3^{Si}Fe–C{\equiv}NH^+$	1.913(3)	1.144(4)	178.4(2)	176(3)
$P_3^{Si}Fe=C=NH$[e]	1.771	1.233	174.4	126.6
$P_3^{Si}Fe–C{\equiv}NMe^+$	1.912(2)	1.157(3)	176.1(2)	176.1(3)
$P_3^{Si}Fe=C=NMe$	1.821(2)	1.186(2)	177.6(1)	150.3(2)
$P_3^{Si}Fe{\equiv}C–N(Me)H^+$[f]	1.751(9)	1.28(1)	169.2(6)	127.6(5)[g]
$P_3^{Si}Fe{\equiv}C\text{-}N(Me)H$[e]	1.689	1.332	175.3	126.5[f]
$P_3^{Si}Fe–NN^+$	1.913(2)	1.091(3)	177.1(2)	*d*
$P_3^{Si}Fe–NN$	1.819(1)	1.124(2)	177.5(1)	*d*
$P_3^{Si}F\text{-}N\ NH^+$[e]	1.684	1.212	176.8	117
$P_3^{Si}Fe–N=NH$[e]	1.675	1.231	177.1	113.8
$P_3^{Si}Fe=N–NH_2^+$	1.672(2)	1.272(3)	175.3(2)	120(3)[h]
$P_3^{Si}Fe=N–NH_2$[e]	1.747	1.294	150.6	122(1)[h]
$P_3^{Si}Fe=N\text{-}N(Me)H^+$	1.671(3)	1.284(4)	174.7(3)	121.6(3)[i]

[a] Measurements are derived from X-ray diffractions studies unless otherwise indicated.

[b] Values in Å.

[c] Values in deg.

[d] Not relevant.

[e] DFT-optimized geometry.

[f] Values taken from predominate disordered isomer.

[g] Refers to C–N–C angle.

[h] Average of two values.

[i] Refers to N–N–C angle.